Transient Lymph Node Immune Activation by Hydrolysable Polycarbonate Nanogels

Christian Czysch, Carolina Medina-Montano, Zifu Zhong, Alexander Fuchs, Judith Stickdorn, Pia Winterwerber, Sascha Schmitt, Kim Deswarte, Marco Raabe, Maximilian Scherger, Francis Combes, Jana De Vrieze, Sabah Kasmi, Niek N. Sandners, Stefan Lienenklaus, Kaloian Koynov, Hans-Joachim Räder, Bart N. Lambrecht, Sunil A. David, Matthias Bros, Hansjörg Schild, Stephan Grabbe, Bruno G. De Geest, and Lutz Nuhn*

The development of controlled biodegradable materials is of fundamental importance in immunodrug delivery to spatiotemporally controlled immune stimulation but avoid systemic inflammatory side effects. Based on this, polycarbonate nanogels are developed as degradable micellar carriers for transient immunoactivation of lymph nodes. An imidazoquinoline-type TLR7/8 agonist is covalently conjugated via reactive ester chemistry to these nanocarriers. The nanogels not only provide access to complete disintegration by the hydrolysable polymer backbone, but also demonstrate a gradual disintegration within several days at physiological conditions (PBS, pH 6.4–7.4, 37 °C). These intrinsic properties limit the lifetime of the carriers but their payload can still be successfully leveraged for immunological studies in vitro on primary immune cells as well as in vivo. For the latter, a spatiotemporal control of immune cell activation in the draining lymph node is found after subcutaneous injection. Overall, these features render polycarbonate nanogels a promising delivery system for transient activation of the immune system in lymph nodes and may consequently become very attractive for further development toward vaccination or cancer immunotherapy. Due to the intrinsic biodegradability combined with the high chemical control during the manufacturing process, these polycarbonate-based nanogels may also be of great importance for clinical translation.

1. Introduction

Targeted immunotherapy offers the opportunity to leverage the specificity and power of the immune system to treat pathologies like viral infections[1] or tumors[2] effectively. For immune engineering, dendritic cells are one of the major interests due to their role as "nature's adjuvant."[3] Dendritic cells are antigen-presenting cells, which orchestrate immunity and activate T cells to execute, e.g., their antitumor effect.[4] One strategy of engineering DCs is to trigger their activation via pattern recognition receptors (PRRs) using small molecular agonists.[5,6] However, preclinical data and clinical trials show the limitation of these compounds.[7,8] Because of unfavorable pharmacokinetic properties, local applications lead to a systemic distribution of PRR agonists such as poly(I:C) (TLR3), imidazoquinolines (TLR7/8), or CpG (TLR9).[9–13] Consequently, immune stimulation and pro-inflammatory cascades are triggered off-target resulting in

C. Czysch, A. Fuchs, J. Stickdorn, P. Winterwerber, S. Schmitt, M. Raabe, M. Scherger, K. Koynov, H.-J. Räder, L. Nuhn
Max Planck Institute for Polymer Research
55128 Mainz, Germany
E-mail: lutz.nuhn@mpip-mainz.mpg.de

C. Medina-Montano, M. Bros, S. Grabbe
Department of Dermatology
University Medical Center of Johannes Gutenberg-University Mainz
55131 Mainz, Germany

Z. Zhong, J. De Vrieze, S. Kasmi, B. G. De Geest
Department of Pharmaceutics and Cancer Research Institute Ghent (CRIG)
Ghent University
9000 Ghent, Belgium

K. Deswarte, B. N. Lambrecht
Department of Internal Medicine and Pediatrics
VIB Center for Inflammation Research
Ghent University
9052 Ghent, Belgium

F. Combes, N. N. Sandners
Laboratory of Gene Therapy
Department of Nutrition
Genetics and Ethology
Ghent University
9820 Merelbeke, Belgium

S. Lienenklaus
Institute for Laboratory Animal Science and Institute of Immunology
Hannover Medical School
30625 Hannover, Germany

severe immune-related toxicities.[14–18] The therapeutic window of these compounds can strongly be enhanced by directing the immune activation to the site of interest or by covalent coupling to solid matrices. The latter approach was lately chosen in the successful development of the TLR7/8 adjuvanted COVID-19 vaccine Covaxin (BBV152), immobilizing an imidazoquinoline derivative to an alum matrix.[19–21] For altering the biodistribution toward the desired target, nanoparticles are especially suitable to serve as carrier systems.[9,10,22,23] Recently, the delivery to immune system sites such as lymph nodes and spleen has shown its potential for successfully engineering the body's immune response.[24–27] For this purpose, various polymeric systems such as poly(meth)acrylates and polynorbonenes have been employed.[23,26,28]

Nonetheless, after successful delivery, a problem remains: Polymeric particles often lack suitable degradability and their clearance from the body is limited.[29] The need for novel degradable materials has stimulated the development of stimuli-responsive materials. These materials are designed by the incorporation of pH or redox-degradable moieties, thus, allowing for disintegration and drug release at the target site.[30–32] However, this approach withholds the fact that a large fraction of particles does not reach the desired target.[33,34] Due to the then lacking external stimulus, these particles remain intact and accumulate in undesired places such as the liver, the lungs, the kidneys, or the spleen.[35] To enhance chemical translatability, materials with a broader range of degradability and an intrinsically limited lifetime are needed to prevent long-term toxicities.[36,37] These criteria could, for instance, be met by nanocarrier systems that gradually hydrolyze in aqueous environment.

Notable examples of hydrolysable architectures are aliphatic polyesters and aliphatic polycarbonates.[36,38–41] Unfortunately, as polyesters degrade, they acidify the surrounding media, which can lead to local tissue irritation and toxicity, limiting their applicability.[42–44] In contrast to that, aliphatic polycarbonates are more promising due to their favorable degradation products. In their case, degradation results in diols and the weak acid carbon dioxide which is unlikely to cause acidification and similar adverse effects.[36,45] Especially, the archetypal poly(trimethylene carbonate) (PTMC) was explored in this regard as a biodegradable and biocompatible implant material.[46–48] However, PTMC is lacking chemical moieties to introduce functionalities. To broaden the scope of applications, a range of functional polycarbonates were designed and investigated as degradable

materials for bioapplications and nanomedicine.[39,49–52] Yet, for most of these structures, degradability was not investigated and just claimed by referring to the degradability of the archetypal, non-functionalized PTMC omitting further analysis to support the hypothesis. So far, it has been shown that polycarbonate degradability can be improved by increasing hydrophilicity.[53–55] The underlying rationale is to increase penetration of water into the structure that should allow for accelerated hydrolysis of the susceptible carbonate moieties. However, not all reported hydrophilic and water-soluble polycarbonates are readily degraded at physiological conditions and further investigations need to provide new insights.[56,57]

We opted for a polymeric carrier system based on aliphatic polycarbonates leveraging their degradability and biocompatibility. In contrast to previous nanogels derived from self-assembling poly(meth)acrylates/-amide or polynorbornene block copolymer micelles, polycarbonates provide unique access to backbone degradability, thus, should prevent long-term toxicological effects that could arise from accumulating materials after therapy.[22,26,58]

Conventional block copolymer micelles that are stabilized by physical (hydrophobic) interactions have limited stability and can disintegrate upon high dilution after injection into the bloodstream.[59] Core-cross-linked systems such as the nanogels of this study circumvent this problem by covalent linkages, strongly avoiding premature block copolymer disassembly.[59–61] Moreover, covalent cross-linking renders the introduction of additional functionalities as well as polarity variation from hydrophobic to hydrophilic inside the core, which is also crucial to enhance degradability. Efficient post-polymerization modification strategies with orthogonal conditions have to be applied to ensure controlled manufacturing. Therefore, we utilized the monomer 5-methyl-5-pentafluorophenyloxycarbonyl-1,3-dioxan-2-one (MTC-PFP) previously described by Hedrick et al. and polymerized it under strong cationic conditions by ring-opening polymerization (ROP), leaving the side-chain untouched and available for post-modification.[57,62,63] By highly increasing the achievable polycarbonate block length, we were able to assemble PEG-based amphiphilic block copolymers into poly(MTC-PFP) micelles and applied them as precursors to generate fully hydrophilic interlinked nanogels. Post-polymerization modification at the active ester side chain[64,65] was employed to conjugate functional primary amines such as fluorescent dyes or the immunostimulatory TLR7/8 agonist IMDQ, while applying non-nucleophilic tertiary amines as catalysts. We here extend this nanogel concept for the first time to polycarbonates and demonstrate that increasing hydrophilicity in polycarbonates indeed allows a gradual degradation at physiological conditions (PBS, pH 6.4–7.4, 37 °C). Investigating the degradation process and its products, the favorable properties of polycarbonate nanogels are shown, bridging toward the biological application as versatile immune-activating carrier systems. The biocompatible properties of the carrier, before as well as after disintegration, were confirmed. Covalent conjugation of the immune-stimulating TLR7/8 agonist IMDQ triggered a localized activation of antigen-presenting cell. As assessed in vitro, the degradation products were even of reduced activity than the intact nanogels, thus, featuring a transient immune stimulation behavior. Moreover, the intact nanogels could well

B. N. Lambrecht
Department of Pulmonary Medicine
Erasmus University Medical Center
3015 Rotterdam, The Netherlands

S. A. David
ViroVax, LLC
Lawrence, KS 66047, USA

H. Schild
Institute of Immunology
University Medical Center of Johannes Gutenberg-University Mainz
55131 Mainz, Germany

L. Nuhn
Macromolecular Chemistry
Department of Chemistry and Pharmacy
Julius Maximilian University Würzburg
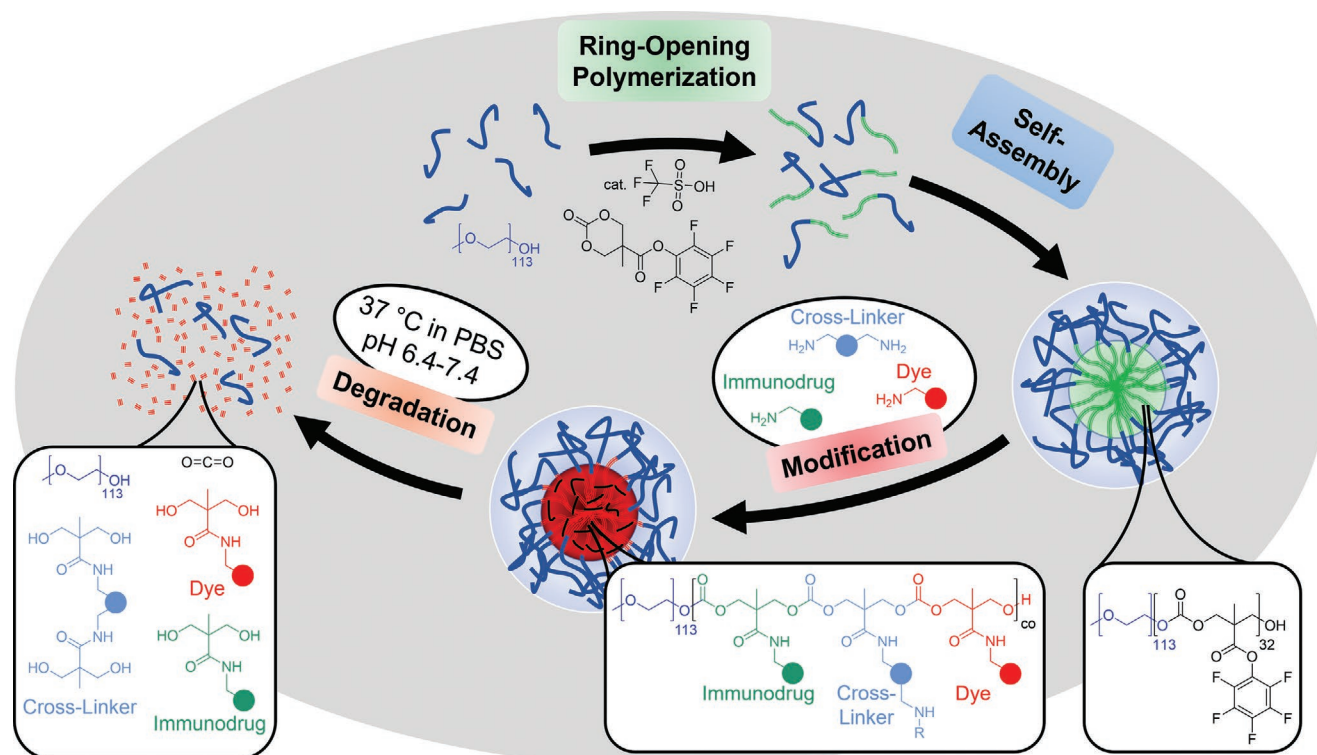97074 Würzburg, Germany

Figure 1. Fabrication of physiologically degradable polycarbonate nanogels. At first, side-chain reactive precursor polymers are produced by ring-opening polymerization. By self-assembly in a block selective solvent, uniform micelles are formed. Upon chemical modification, drug, dye, and cross-linking units are introduced, yielding fully hydrophilic nanogels. Those gels are hydrolytically degradable at body temperature in PBS (pH 6.4–7.4) showing both a pH- and a temperature-dependent degradation behavior.

drain to the lymph nodes and initiate a spatially controlled maturation of antigen-presenting cells while avoiding systemic off-target immune overstimulation. Altogether, the hydrolysable polycarbonate nanogel platform (**Figure 1**) provides beneficial features to improve the pharmacokinetics of immune-stimulatory drugs and guarantees their transient delivery into antigen-presenting cells in draining lymph nodes.

2. Results and Discussion

2.1. Synthesis of mPEG-Polycarbonate Block Copolymers

5-Methyl-5-pentafluorophenyloxycarbonyl-1,3-dioxan-2-one (MTC-PFP) can be conveniently synthesized in a one-step reaction starting from 2,2-bis(hydroxymethyl)propionic acid (Bis-MPA) by cyclization of the six-membered carbonate and esterification of the carboxylate group (**Figure 2**A; Figures S1–S3, Supporting Information).[66] For subsequent polymerization of MTC-PFP, we realized that it has to be of exceptional purity to achieve high block lengths and control over the polymerization. Since residual diols or other nucleophilic impurities would act as unwanted initiators, the product was recrystallized two times from a hexane/ethyl acetate mixture yielding colorless needles. Exceptional quality was confirmed by X-ray diffraction analysis that also gained insights into the molecular conformation (Figure 2A; Figure S1, Supporting Information). From the crystallographic data, it can be seen that the methyl side group

and the pentafluorophenyl ring system are in proximity which potentially contributes to the high ring-opening polymerization reactivity by steric repulsion. In-depth analysis of the monomer by 2D NMR further demonstrated the high purity of the compound (Figures S2 and S3, Supporting Information).

In view of the requirements for bioapplications, polycarbonates were generated using an organocatalyst system.[67] By these means, the use of conventional metal-based catalysts should be avoided, as such potentially toxic compounds would hamper both safe application and regulatory acceptance of the material.[68] To this end, the amphiphilic block copolymers mPEG$_{113}$-b-poly(MTC-PFP) were synthesized by cationic ring-opening polymerization using trifluoromethanesulfonic acid (Figure 2A). High selectivity of this organocatalyst for the ring-opening reaction over side chain reaction has already been reported by Hedrick et al. using mPEG$_{113}$-OH as macroinitiator.[63,67] However, previously only short block lengths were achieved for block copolymers.[63] We observed that these block lengths are insufficient for the self-assembly of polymeric micelles and that the respective polymers remain molecularly soluble (Figure S9, Supporting Information). Yet, to employ these polymers as a platform for polymer analogous reactions within the resulting micelle cores, the polymerization technique had to be optimized toward increasing the polycarbonate block length. Using higher dilutions of the monomer at 0.5 m combined with a low catalyst loading, thoroughly drying all starting materials by azeotropic distillation, and applying water-free conditions in a nitrogen-purged glove box, polymers of a block length of ≈32 units were
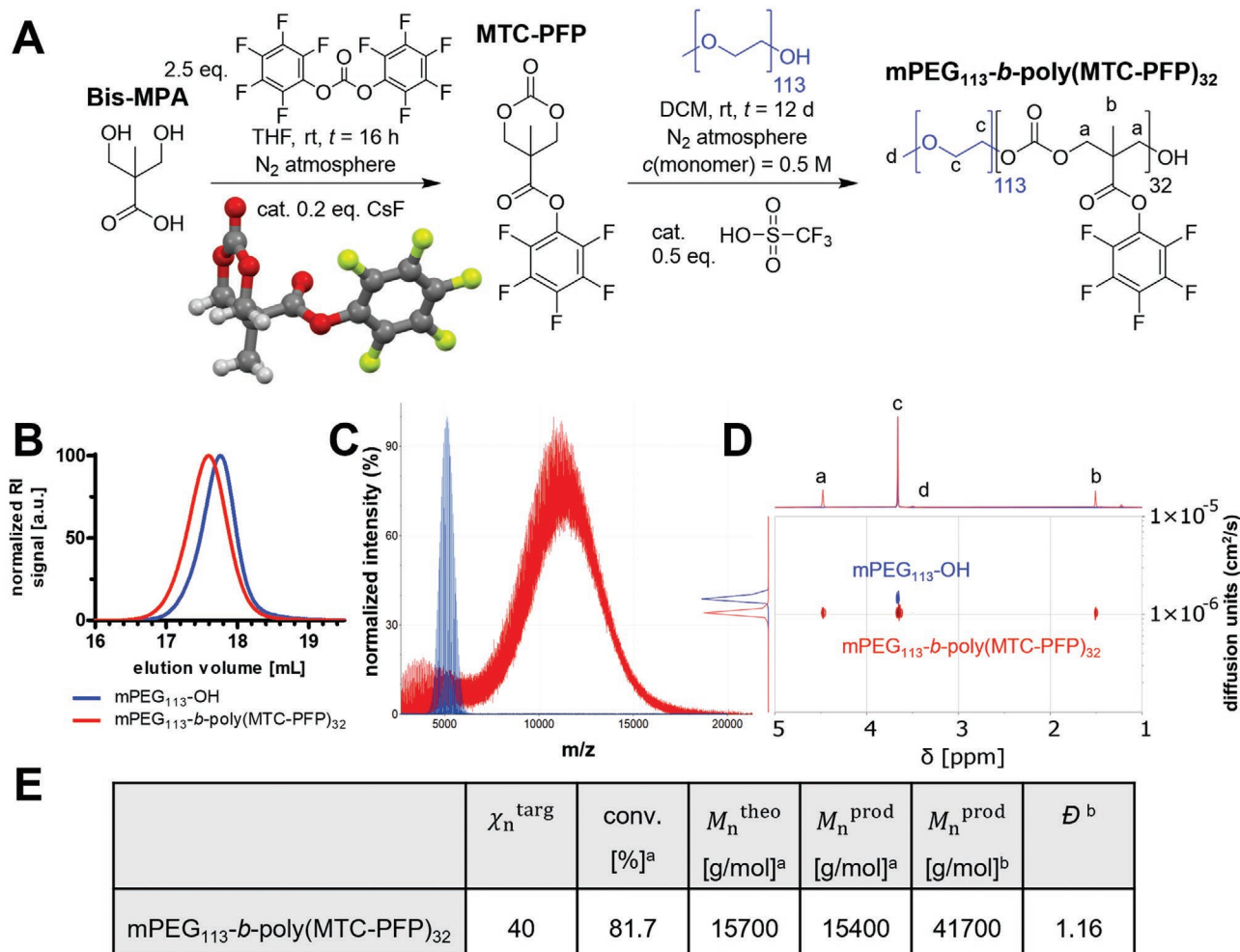
Figure 2. Synthesis and characterization of polycarbonate-based reactive precursor polymers. A) Reaction scheme of monomer and block copolymer synthesis. 5-Methyl-5-pentafluorophenyloxycarbonyl-1,3-dioxan-2-one one (MTC-PFP) was yielded from the reaction of 2,2-bis(hydroxymethyl)propionic acid with bis(pentafluorophenyl)carbonate by simultaneous carbonate cyclization and side group esterification reaction. The X-ray diffraction analysis derived crystal structure of the MTC-PFP monomer is provided as well (further information can be found in Figure S1, Supporting Information). Polymerization was afterward initiated from polyethylene glycol using trifluoromethanesulfonic acid as organocatalyst. B) Size exclusion chromatography (SEC) elugram of mPEG$_{113}$-b-poly(MTC-PFP)$_{32}$ (red) and mPEG$_{113}$-OH (blue) showing successful block copolymer formation by a shift toward higher mass (lower retention time) and a monomodal distribution (Đ = 1.16). C) Mass spectrometric analysis of mPEG$_{113}$-OH (blue) and mPEG$_{113}$-b-poly(MTC-PFP)$_{32}$ (red). The block copolymer shifts toward higher molecular mass and contains no polycarbonate or mPEG$_{113}$-OH homopolymers. D) Diffusion Ordered Spectroscopy (DOSY) NMR of mPEG$_{113}$-OH macroinitiator (blue) and mPEG$_{113}$-b-poly(MTC-PFP)$_{32}$ block copolymer (red). For the latter, all signals appear at a larger diffusion coefficient indicating the purity of the block copolymer. E) Summary of the analytical results for mPEG$_{113}$-b-poly(MTC-PFP)$_{32}$. [a]Determined by ^{1}H NMR analysis; [b]Determined by SEC with HFIP (hexafluoroisopropanol) as eluent and calibration with PMMA standards.

yielded (Figure 2A,E; Figure S4–S8, Supporting Information). For polymer purification, the reaction mixtures were precipitated into ice-cold diethyl ether, decanted, and dried in vacuo. Successful grafting of the polycarbonate block to the polyethylene glycol macroinitiator was confirmed by size exclusion chromatography (SEC). The elugram (Figure 2B) shows a monomodal size distribution and a shift toward higher molecular mass, relative to the polyethylene glycol macroinitiator (Đ = 1.16). This finding was further supported by ^{1}H diffusion ordered NMR spectroscopy (^{1}H DOSY NMR) (Figure 2D) showing only one single diffusing species with polycarbonate and polyethylene glycol signals at higher diffusion units compared to the mPEG$_{113}$-OH macroinitiator. Moreover, mass spectrometry

nicely demonstrated successful grafting of the carbonate block as well as the absence of homopolymers (Figure 2C—for detailed analysis compare Figures S5 and S6, Supporting Information).

2.2. Fabrication of Immunostimulatory Polycarbonate Nanogels

After successfully establishing a procedure for obtaining suitable polycarbonate block lengths, the polymers' self-assembly behavior was investigated (**Figure 3**A). Ethanol was selected as organic solvent in which PEG is fairly soluble, but the poly(MTC-PFP) block remains insoluble. Supported by ultrasonication the block copolymers were redispersed
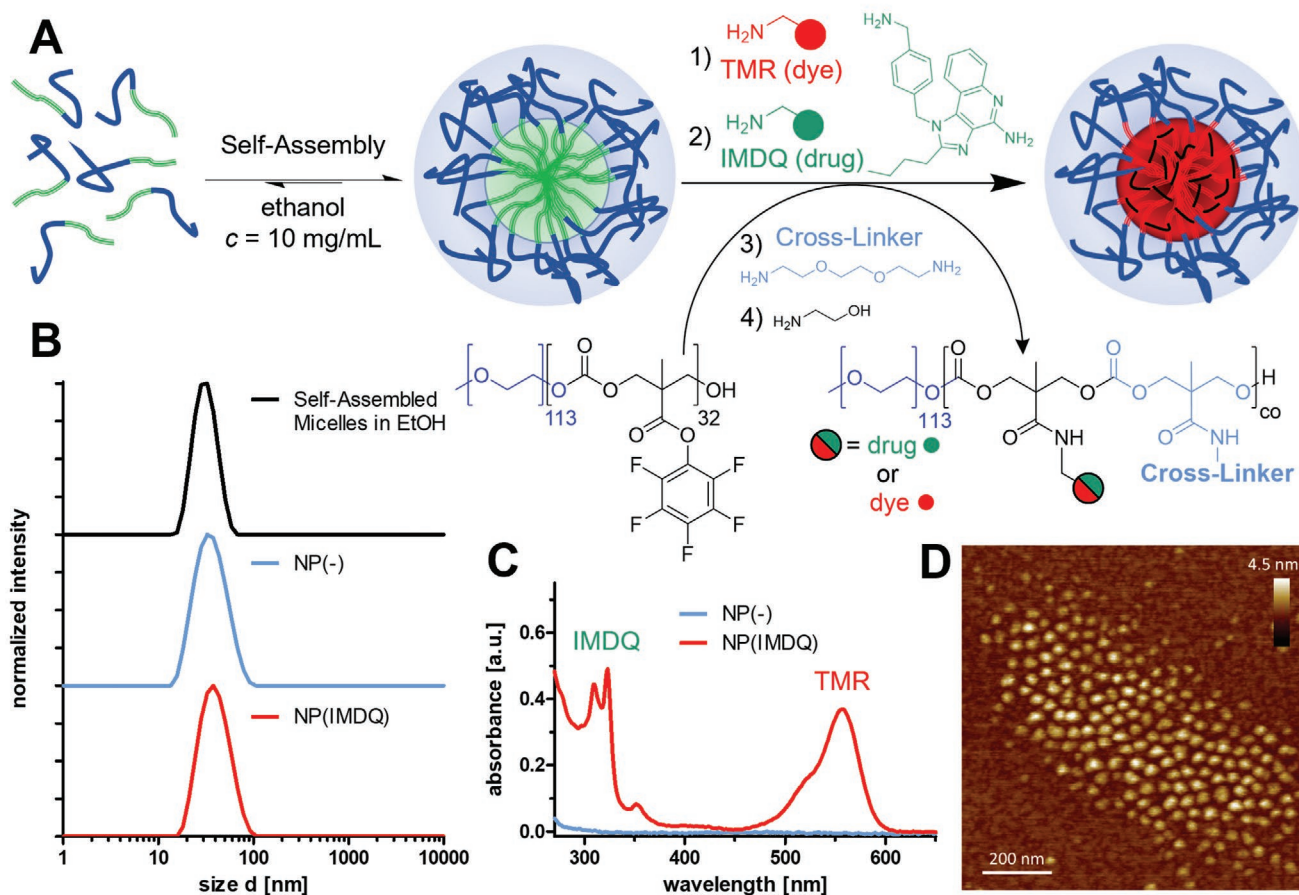
ADVANCED
SCIENCE NEWS
www.advancedsciencenews.com

ADVANCED
FUNCTIONAL
MATERIALS
www.afm-journal.de

Figure 3. Fabrication of immunodrug-loaded polycarbonate nanogels. A) Reaction scheme for the synthesis of the polycarbonate nanogels. Self-assembly of mPEG$_{113}$-b-poly(MTC-PFP)$_{32}$ block copolymer could be achieved in the PEG block selective solvent ethanol supported by ultra-sonification, followed by the chemical modification of these precursor micelles into nanogels. Simultaneous core functionalization was obtained by aminolysis with amine-containing fluorescent dyes (TMR) and immune stimulatory drugs (IMDQ) prior to cross-linking with a hydrophilic bis-amine. Finally, an excess of ethanolamine was added to quench the remaining pentafluorophenyl esters. B) DLS analysis of the self-assembled precursor micelles and of the resulting core-cross-linked nanogels. Both show comparable hydrodynamic diameters (29.9, 32.4, and 36.2 nm for precursor micelles, nanogels and drug-loaded nanogels) and monomodal size distributions (PDI = 0.06, 0.06, and 0.14 for precursor micelles, nanogels and drug-loaded nanogels). C) UV–vis absorbance spectra of non-loaded (blue) versus drug- and dye-loaded nanogels (red). Covalent dye and drug conjugation results in additional absorption maxima at 550 (TMR absorption) and 321 nm (IMDQ absorption) from which the drug-load was determined (compare Figure S14, Supporting Information). D) AFM image of core-cross-linked nanogels dried on flat mica surfaces showing uniform particles with flattened heights of ≈2 nm and similar diameters of ≈33 nm (compare Figures S12 and S13, Supporting Information).

in that solution and then characterized by dynamic light scattering (DLS). When polymers with short polycarbonate block lengths were utilized, polymer chains remained in the solution and did not self-assembly into micelles (Figure S9, Supporting Information). Monodisperse micellar particles were only gained for larger poly(MTC-PFP) blocks, e.g., with mPEG$_{113}$-b-poly(MTC-PFP)$_{32}$ in ethanol as analyzed by DLS in Figure 3B. These polymeric micelles were then functionalized using primary amines. They can react with the activated pentafluorophenyl esters and form stable amide bonds. By these means, cargo molecules such as fluorescent tracer molecules (e.g., tetramethyl rhodamine cadaverine (TMR)) or immunostimulatory drugs (e.g., the TLR 7/8 agonist IMDQ) were covalently attached to the polymeric chains (Figure 3A). We followed previously reported protocols for covalent cargo molecule conjugation to self-assembled pentafluorophenyl ester

block copolymers,[22,23] and subsequently core-crosslinked the remaining activated esters inside the particles using the hydrophilic bisamine 1,8-diamino-3,6-dioxaoctane. Finally, to ensure that no residual perfluorinated active esters were present in the product, the thereby obtained nanogels were quenched by addition of excess ethanolamine affording fully hydrophilic cores. The reaction conversion was analyzed by ^{19}F NMR which is an ideal technique for this purpose due to low detection limit of ^{19}F and high specificity[69] (compare Figure S11, Supporting Information). Indeed, it was confirmed that these conjugation reactions proceeded to quantitative conversions even within several minutes. For particle functionalization a reaction time of 30 min was chosen to ensure complete conversion in the dense polymeric network. Subsequently, the reaction mixtures were added to 1 M hydrochloric acid to avoid an alkaline pH, which would trigger carbonate hydrolysis and

loss of yield during the following dialyses steps. Side products, unreacted amines, and salts were removed by frequent exchange of water (pH 4). Afterward, the solutions were lyophilized to obtain nanogels as a voluminous powder that allowed long-term storage in the dried state.

Due to the highly hydrophilic properties, the lyophilized material could quickly be redissolved in water to provide fresh batches of nanogel solution. Notably, nanogel particles were obtained with comparable size to the initially self-assembled polymeric micelles in ethanol even after redispersion: Particle sizing by dynamic light scattering (DLS, Figure 3B) gave monodisperse particles with hydrodynamic diameters of 32.4 nm and a narrow dispersities (PDI = 0.06), while their respective precursor micelles provided sizes of 29.9 nm and PDI = 0.06 in ethanol (covalent IMDQ drug loading only marginally increased the size of the nanogels 36.2 nm at a PDI = 0.14, compare Figure S10, Supporting Information—for additional multi-angle DLS, compare Figure S20, Supporting Information). The fully converted nanogels yielded a neutral zeta-potential (Figure S12, Supporting Information), while atomic force microscopy (AFM) images of nanogels deposited on flat mica surfaces visualized their homogenous spherical shapes (Figure 3D), and thus confirmed the successful covalent cross-linking of the self-assembled block copolymers (statistical analysis of the recorded AFM images confirmed the remarkably narrow particle size distribution—compare Figures S12 and S13, Supporting Information). To precisely quantify fluorescent dye loading and—more importantly for therapeutical applications—the immunodrug loading, these covalently immobilized functional groups could be quantified by UV–vis absorbance measurements (Figure 3C). For IMDQ, a calibration curve was applied using the specific UV absorption of the drug compound ≈321 nm yielding an IMDQ-load of ≈6.5 wt.% (compare Figure S14, Supporting Information).

2.3. Behavior of Polycarbonate Nanogels at Physiological Conditions

Aliphatic polycarbonates are a class of materials that are reported to be hydrolytically degradable, however, detailed identification of the degradation products is often overlooked. Moreover, degradation kinetics providing important information on the degradation conditions and the related timescales are missing. Yet, they are relevant to apply the material for instance in vivo. Especially for fine-tuned applications like nanocarrier-guided immunotherapies, it is of major importance to not only trigger immune responses but also to terminate the activation in order to avoid severe over-activation followed by auto-immunity.[14,15] In view of drug safety regulation and translatability of polymeric drug delivery systems, long-term accumulation of the polymeric material and respective degradation products have to be avoided.[70,71]

With this in mind, we investigated the hydrolytic degradation profile of the hydrophilic nanogels (**Figure 4**A) using several complementary techniques, including dynamic light scattering (DLS), fluorescence correlation spectroscopy (FCS), NMR spectroscopy, and mass spectrometry. According to the IUPAC definition, materials are described as "hydro-degradable" if they disintegrate upon action of water.[72] Since hydrolytic

degradation strongly depends on the pH, we first investigated its influence on the hydrolysis of polycarbonate nanogels. Hence, nanogels were redispersed and diluted to respective pH values followed by incubation at 37 °C for several days (Figure 4B, for respective size distributions, compare Figure S16, Supporting Information). They were measured frequently by DLS to gain information about the size and the scattering count rate (the latter can be seen as a proximation for the particle concentration). It was observed that nanogels remained exclusively stable over a period of several weeks at non-physiological acidic pH of 4.0 or 5.5 (Figure 4B1). This would allow nanogel storage at such pH values in aqueous media. In stark contrast, rapid degradation was observed in alkaline media at pH 9.0 by immediate decreasing sizes and count rates (a half-life of ≈3 h was estimated—compare Figure S17, Supporting Information). Most notably, the sample incubated in PBS of pH 7.4 at 37 °C showed also gradual particle disintegration with a scattering count rate half-life of ≈24 h (Figure 4B1—compare Figure S17, Supporting Information). This half-life time is still sufficient to ensure sample stability for a reasonable period for in vitro or in vivo applications at 37 °C. The behavior of particles to remain stable before decaying is an important feature for avoiding long-term toxicological effects as well as for timed immune stimulation. Additionally, we also observed a gradual but slower decay at physiological acidic pH values of 6.4 and 6.8 (with half-life of 66 and 30 h, respectively, Figure 4B1; Figure S17, Supporting Information) that can be found in lymph nodes[73] and tumor sites.[74,75] Thus, even at those locations a clearance of nanogels by hydrolytic disintegration can still occur. Interestingly, polycarbonate nanogels also show a temperature-dependent degradation profile as demonstrated by prolonged stability at 4 °C even after several weeks (Figure 4B2, compare Figure S18, Supporting Information for half-life times). Consequently, polycarbonate nanogel degradation does not only depend on pH but can also be controlled at physiological conditions by temperature. This further provides an ideal storage possibility in solution at 4 °C but excludes possible long-term accumulation effects upon application within a biological system at 37 °C.

Additionally, degradation was analyzed by fluorescence correlation spectroscopy (FCS), which is a method to provide size information of fluorescently labeled material (Figure 4C). Thereby, the small molecular fluorescence dye TMR, which was covalently immobilized inside the nanogels, was tracked. Its degradative release was observed over time and served as a model for the release of covalently attached drug molecules. The dye-labeled nanogels were incubated in PBS at 37 °C and the related autocorrelation functions were recorded at several time points (Figure 4C1). In the beginning, most of the dye molecules were attached to the particles providing an average hydrodynamic diameter of 32.8 nm, in analogy to the previous DLS measurements. Over time, an increasing amount of released fluorescent dye was detected (Figure 4C3), while the size of the nanogel also gradually decreased (Figure 4C2). From the release kinetics of the fluorescent dye, a half-life of ≈54 h could be determined that is in a similar regime as obtained previously (we assume that the slightly larger half-life is probably due to some dye entrapment inside the degrading nanogel—compare Figure S19, Supporting Information). Approximately after 3 days, most of the dye was released that assures sufficient time for delivery of
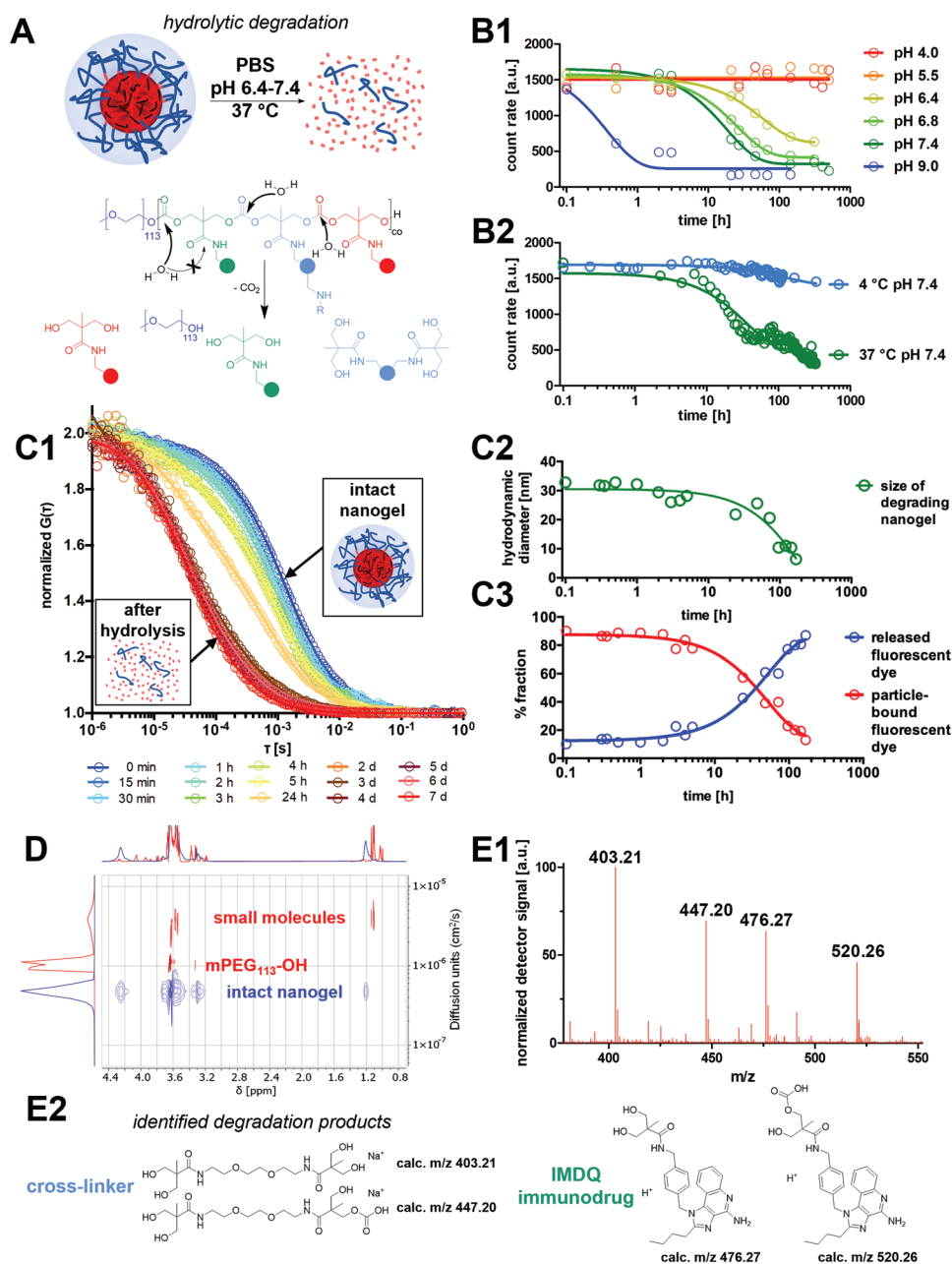
Figure 4. Gradual degradation of polycarbonate nanogels under physiological conditions. A) Hydrolytic cleavage of the polycarbonate nanogels with the expected degradation products: hydrophilic diols, carbon dioxide, and polyethylene glycol. B) pH (1) and temperature (2) dependent degradation monitored by DLS. Under degradation triggering conditions particle sizes and scattering count rates drop. C) FCS degradation kinetics of TMR-labeled nanogels in PBS (37 °C) monitored by the corresponding autocorrelation functions (1) followed by the fit-derived remaining hydrodynamic nanogel diameter (2) and the fractions (3) of particle-bound and released fluorescent dye. D) Release of small molecules and mPEG$_{113}$-OH (red) from the nanogel's network (blue) investigated by ^{1}H DOSY NMR measurements (PBS, pH 7.4). E1) Recorded ESI-MS spectrum after nanogel degradation. E2) Identified degradation products according to the recorded ESI-MS spectrum confirming respective diol product formation.

the carrier system during bioapplications. Degradation of polycarbonate nanogels yields small-molecular weight dye molecules, which distinguishes the polycarbonate-based systems from earlier nanogel systems where degradability was introduced by pH-degradable crosslinkers. The pH-triggered particle unfolding results in single soluble polymer chains that are still covalently equipped with the fluorescent dye or drug.[76–78] For

the polycarbonate nanogels introduced in this study, hydrolytic degradation affects the polymeric backbone yielding small molecular weight hydrolysis products (that are assumed to have easier access to metabolic recovery or renal clearance). To study the hydrolysis products in more detail, we next applied NMR spectroscopy and mass spectrometry to identify the molecular structures formed during nanogel degradation.

Drastic size changes and generation of small degradation products were observed in liquid ^{1}H DOSY NMR. Nanogels were diluted in deuterated water and detectable as a single slow diffusing, high molecular weight species (Figure 4D). Upon addition of PBS and incubation at 37 °C for a prolonged time, novel low molecular species were released from the high molecular nanogel (compare Figure S22, Supporting Information). Ultimately, the polymeric particles' signal shifted toward higher diffusion coefficients, and signals of the polycarbonate backbone vanished. This strongly indicates the degradation of polycarbonate backbone, which is contrasted by the stability of polyethylene glycol that was still found as polymeric species by ^{1}H DOSY NMR. In conclusion, it was shown that small molecular species were released from nanogel networks during degradation at the relevant physiological conditions. High-Resolution Magic Angle Spinning (HRMAS) ^{1}H NMR measurements were performed to get further insights into the processes that occur within the densely interlinked nanogel core (compare Figure S23, Supporting Information—note that conventional ^{1}H NMR was less reliable for quantification purposes). Upon addition of PBS and incubation at 37 °C for prolonged time, degradation of the polycarbonate backbone was observed, as can be seen by the slow decline of signals of the methyl sidechain as well as the methylene groups of the backbone. Most significantly, the amide bonds remained untouched which nicely shows the higher stability of these linkages compared to the susceptible carbonate backbone: During degradation amide signal integral remained unchanged, indicating that no reactions are taking place at the side chain (Figure S23, Supporting Information). Kinetic evaluation of the degradation process by HRMAS revealed comparable half-life degradation values to FCS and DLS in PBS (Figure S24, Supporting Information) and thus implied that indeed the molecular process of polycarbonate backbone disintegration triggers the particle disassembly.

Finally, mass spectrometry was employed to ultimately identify the small molecular degradation products, as highlighted in Figure 4A. First, electrospray ionization mass spectrometry (ESI-MS) was applied to aqueous solutions of nanogels incubated for several days at 37 °C in a 1:100 water/triethylamine solution (to ensure full degradation in the presence of volatile salts/molecules that are tolerable for ESI-MS measurements). Indeed, analysis of the recorded spectra confirmed the diolic derivates of the cross-linker (m/z = 403.21) as well as the drug compound (m/z = 476.27) as main species (Figure 4E1,E2; Figure S25, Supporting Information). Thereby, it was not only confirmed that the carbonate backbone is more susceptible than the amide side chains, but also additional side reactions that could have occurred during nanogel synthesis could be excluded (e.g., PFP hydrolysis or transesterification with ethanol, as none of the afforded by-products could be found either). In addition, matrix-assisted laser desorption/ionization (MALDI) MS spectra were recorded to analyze the molecular architecture of the residual polymeric degradation products after incubation in PBS at 37 °C for 2 weeks. While the initial precursor block copolymers provided a molecular weight of ≈15 kDa (Figure 2D), the nanogels after degradation provided again polymeric material with a mass of ≈5 kDa, which exactly matched with the mass of the initially used polyethylene glycol homopolymer (compare Figure S26, Supporting Information). Again, it could be confirmed that a full degradation of polycarbonate nanogels under physiological conditions leads to hydrophilic diols and renally clearable polyethylene glycol,[79] making it an ideal degradable carrier system for biological application. The intrinsically limited lifetime of polycarbonate nanogels at physiological conditions can prevent long-term toxicity but provides a high temporal control over immunotherapeutic stimulation.

Prior to further in vitro and in vivo investigations, we were also interested in the behavior of the intact nanogel exposed to complex biological media. Therefore, particle stability in physiological relevant protein-rich conditions was investigated by incubation in human blood plasma for 1 h at 37 °C, followed by a multi-angle light scattering analysis to test for potential polymer-protein-aggregates (Figure S21, Supporting Information). By this well-established method,[80] no significant differences of recorded and predicted autocorrelation curves were found, indicating that the nanogels with or without IMDQ do not aggregate upon protein incubation but remain stable.

2.4. In Vitro Performance of Immunostimulatory Nanogels

In-depth characterization of the covalently functionalized polycarbonate nanogels as well as their favorable transient degradation profile suggested their suitability for further developments toward biological application. Initial in vitro tests focused on the cellular toxicological profile of the polycarbonate nanogels and confirmed their high biocompatible properties. Cell viability of empty and drug-loaded nanogels NP(-) and NP(IMDQ) was not impaired across a broad range of concentrations up to >0.5 mg mL^{-1} on macrophages (Raw Blue cell line) (**Figure 5**A). Next, nanogel uptake was investigated by incubation of macrophages with fluorescent dye-labeled nanogels (compare Figure S15, Supporting Information for the nanogels' fluorescence emission properties). Flow cytometry showed a concentration-dependent particle uptake (Figure 5B as well as Figures S27 and S28, Supporting Information). Interestingly, compared to empty nanogels NP(-), the uptake of the IMDQ-loaded particles NP(IMDQ) was significantly higher (Figure 5B; Figure S28, Supporting Information). Similar results were obtained by confocal microscopy confirming the internalization, especially of the drug-loaded particles (Figure 5C; Figures S29 and S30, Supporting Information). This preferential uptake could probably be triggered by the immunostimulatory effect of the nanogels' payload.

To investigate IMDQ-mediated TLR7/8 receptor stimulation, the reporter function of macrophages (Raw Blue cell line) was applied. These cells have been genetically engineered to express alkaline phosphatase in response to NF-κB activation. Secreted alkaline phosphatase can subsequently be quantified spectrophotometrically in the cell culture supernatant by the Quanti Blue assay. By screening a broad range of concentrations, the NF-κB inducing activity of the highly potent soluble IMDQ (sIMDQ) increased from lower to higher nanomolar range when conjugated to the nanogel, while the empty nanogel induced no NF-κB activity and, thus, remained immunologically silent (Figure 5D). We also studied the degraded
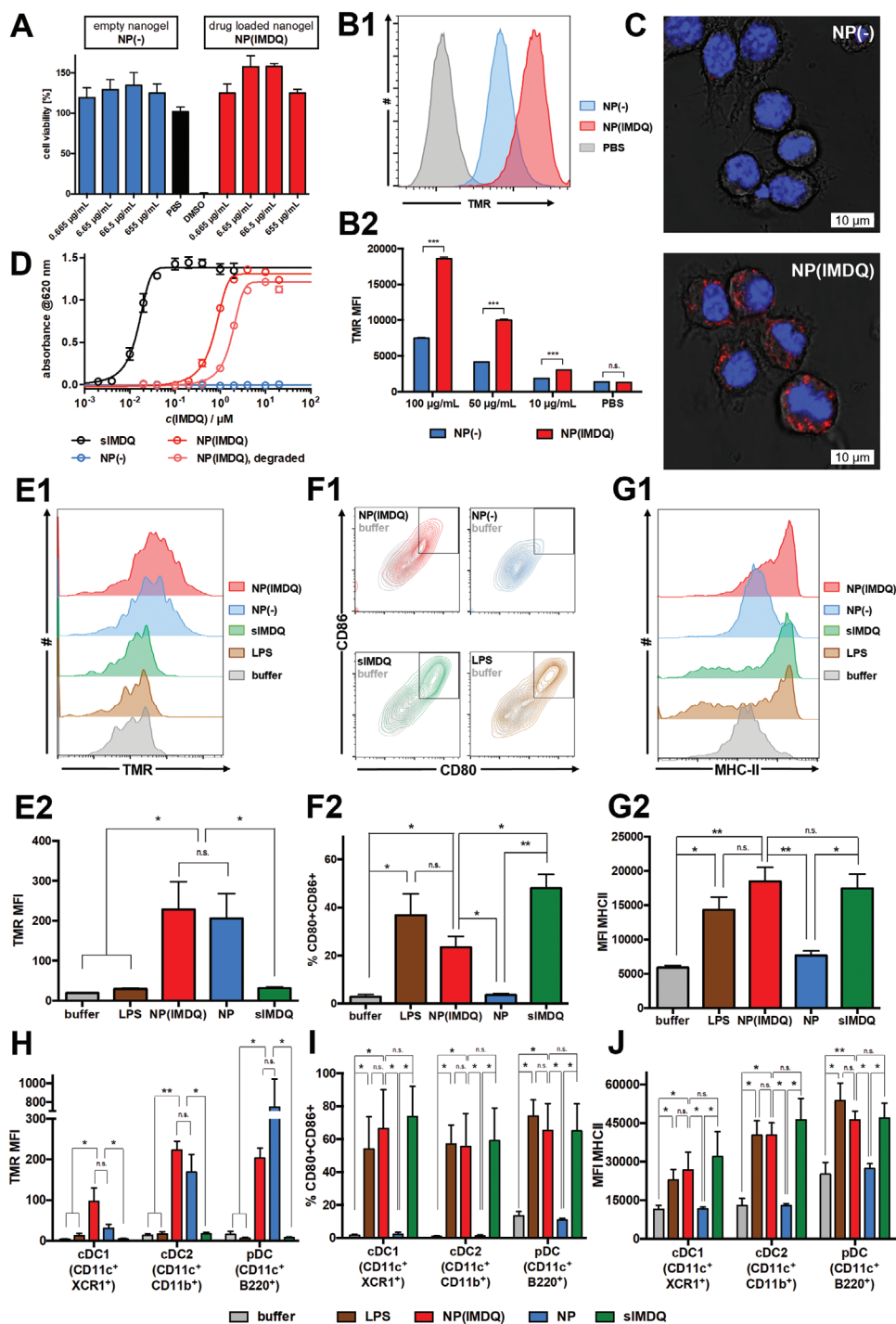
2203490 (8 of 14)

Figure 5. In vitro evaluation of immunodrug-loaded polycarbonate nanogels. A) Cell viability testing by MTT-Assay indicates high compatibility over a broad concentration range in Raw Blue Macrophages ($n = 4$). B) Cell uptake of TMR-labeled nanogels in Raw Blue macrophages quantified by flow cytometry histogram (1) or mean fluorescence intensity (MFI) (2) analysis ($n = 3$). C) Cell internalization could be confirmed by confocal microscopy of RAW Blue macrophages incubated with TMR-labeled nanogels (red) and nuclei stained with DAPI (blue). D) TLR7/8 activation of RAW Blue macrophages quantified by Quanti Blue assay of cell culture supernatant ($n = 4$). E) Cell uptake of TMR-labeled nanogels in GM-CSF derived BMDCs analyzed by flow cytometry histogram (1) or mean fluorescence intensities (MFI) (2) ($n = 4$). F) CD80 and CD86 expression of GM-CSF derived BMDCs analyzed by flow cytometry histogram (1) or mean fluorescence intensities (MFI) (2) ($n = 4$). G) MHCII expression of GM-CSF derived BMDCs analyzed by flow cytometry histogram (1) or mean fluorescence intensities (MFI) (2) ($n = 4$). H) Cell uptake of TMR-labeled nanogels in Flt3 ligand derived BMDC subpopulations analyzed by flow cytometry MFI ($n = 3$). I) CD80 and CD86 expression of Flt3 ligand derived BMDC subpopulations analyzed by flow cytometry MFI ($n = 3$). J) MHCII expression of Flt3 ligand derived BMDC subpopulations analyzed by flow cytometry MFI ($n = 3$; $^*p \leq 0.05$; $^{**}p \leq 0.01$; n.s.: not significant).

NP(IMDQ) after complete nanogel hydrolysis and found a further reduced immune stimulatory activity with a shift into the micromolar regime. Similar effects have been reported by us for polynorbornene-derived nanogels covalently functionalized with IMDQ.[28] Upon pH-triggered nanogel unfolding, a reduction of the TLR7/8 receptor activation was found there, too, and thus suggested a suitable clinical safety profile for both systems: Their degradation products not only circumvent non-favorable nanoparticle accumulation in the body, but also provide less active IMDQ species. Only the intact nanogel carriers seems to support sufficient IMDQ's receptor stimulation (probably by enforced endosomal internalization), while unwanted systemic immune activation is reduced after particle disintegration.

To further evaluate the immunostimulatory profile of the intact polycarbonate nanogels loaded with IMDQ, we investigated their behavior on primary dendritic cells differentiated from murine bone marrow. Upon differentiation in the presence of GM-CSF supplemented media, inflammatory bone-marrow-derived dendritic cells (BMDCs) were obtained and incubated overnight with empty and IMDQ-loaded nanogels, as well as soluble IMDQ and the TLR4 agonist LPS as a control (Figure 5E–G). By flow cytometric analysis (Figure S31, Supporting Information), binding of both particles NP(-) and NP(IMDQ) was observed (Figure 5E). However, a difference in terms of binding or uptake between the two particle species could not be found (compared to the macrophage cell line in Figure 5B,C).

We also checked for the immunostimulatory phenotype on these BMDCs and determined the surface expression of the costimulatory molecules CD80 and CD86 as relevant markers for dendritic cell maturation (Figure 5F). While the empty nanogels NP(-) again exerted no stimulatory effect (like the buffer control), the covalently attached IMDQ inside the nanogels NP(IMDQ) triggered simultaneous upregulation of both maturation markers, as observed for sIMDQ and LPS. Likewise, the antigen presenting receptor MHCII was strongly upregulated in response to treatment with NP(IMDQ), at similar extent as evoked by sIMDQ and LPS (Figure 5G). Altogether, these observations underline the particles' immune stimulatory potential on primary immune cells.

Murine bone marrow cells can also be used to differentiate into different dendritic cell subpopulations by applying Flt3 ligand supplemented media. By this means, conventional (myeloid) dendritic cells cDC1 (CD11c$^+$ XCR1$^+$) and cDC2 (CD11c$^+$ CD11b$^+$) as well as plasmacytoid dendritic cells pDC (CD11c$^+$ B220$^+$) are obtained (compare Figure S32, Supporting Information). cDC1 cells are considered to preferentially induce type 1 immune responses yielding cytotoxic T cells that kill infected and malignant cells.[81] cDC2 preferably induces type 2 immune responses that are directed against parasites and bacteria.[82] pDCs are renowned for their high type 1 interferon secretion and pronounced antigen presentation capacity, especially in the context of viral infections.[83,84] Similar to inflammatory BMDC induced by GM-CSF, Flt3 ligand differentiated BMDC, comprising a mixture of cDC1/2 and pDC, were again incubated for 24 h with empty and IMDQ-loaded nanogels, as well as soluble IMDQ and LPS as control and afterward analyzed by flow cytometry (Figure S32, Supporting Information). Nanogel

uptake could be monitored by TMR fluorescence in those different subtypes. Again, no significant difference between NP(–) and NP(IMDQ) was observed in all dendritic cell populations, although particle uptake seemed to be slightly higher in cDC1 for IMDQ-loaded nanogels than empty nanogels, while the reverse observation could be made in pDC (Figure 5H; Figure S33, Supporting Information). We also checked the maturation status of all three dendritic cell subtypes. In agreement with our previous observations on the GM-CSF induced BMDCs, the empty nanogel NP(-) behaved immunologically silent like the buffer control, whereas the nanogel-bound IMDQ samples NP(IMDQ) triggered simultaneous upregulation of both co-stimulatory maturation markers CD80 and CD86 in cDC1, cDC2, and pDC cells (Figure 5I; Figure S33, Supporting Information). Similar levels could also be obtained for sIMDQ and LPS. Moreover, in all three dendritic cell subtypes, the expression of MHCII was also further stimulated for differentially stimulated samples, including the treatment with NP(IMDQ) (Figure 5J; Figure S33, Supporting Information). These findings underline the pronounced nanogels' potential to retain the drugs' immune-stimulatory performance on various immune cells when covalently attached to the hydrolysable nanogel carrier.

2.5. In Vivo Performance of Immunostimulatory Nanogels for Lymph Node-Targeted Delivery

Following these promising in vitro results on cultured cell lines and primary immune cells, we were interested in the nanogels' in vivo applicability. In previous reports, we could demonstrate that various types of macromolecular carriers can spatiotemporally control the delivery of covalently attached IMDQ while omitting the drug's systemic inflammatory off-target effects.[22,26,85–89] Giving the fact that the empty nanogel NP(–) remained immunologically silent during the in vitro experiments, we therefore administered the IMDQ-nanogel NP(IMDQ) versus the soluble drug sIMDQ subcutaneously into the footpad of mice. We aimed for a focused delivery of the nanogels to the draining lymph nodes followed by a local activation of lymph node residing and infiltrating immune cells while excluding a systemic activation of immune system. A visualization of the immune cell activation can be performed in IFN-β luciferase reporter (IFN-$\beta^{+/\Delta\beta\text{-luc}}$) mice that provide local bioluminescence upon stimulation of IFN-β secretion.

We monitored the bioluminescence for 48 h (**Figure 6**A; Figure S34, Supporting Information) and indeed observed a local activation upon NP(IMDQ) footpad injection in the draining popliteal lymph node while injection of the soluble drug sIMDQ led to distribution all over the body and caused severe systemic inflammations that prolonged for 24 h and then gradually decreased after 48 h. For the nanogels, however, beyond some luciferase liver background signal that was also found before injection ($t = 0$ h) (Figure 6A) or in the buffer control (Figure S34, Supporting Information), a pronounced signal was found only in the local lymph node, especially at 4 h. It also gradually decayed over time, which goes along well with hydrolytic degradation profile of the hydrolysable polycarbonate nanogels (compare Figure 4) affording less immunostimulatory by-products (compare Figure 5D).
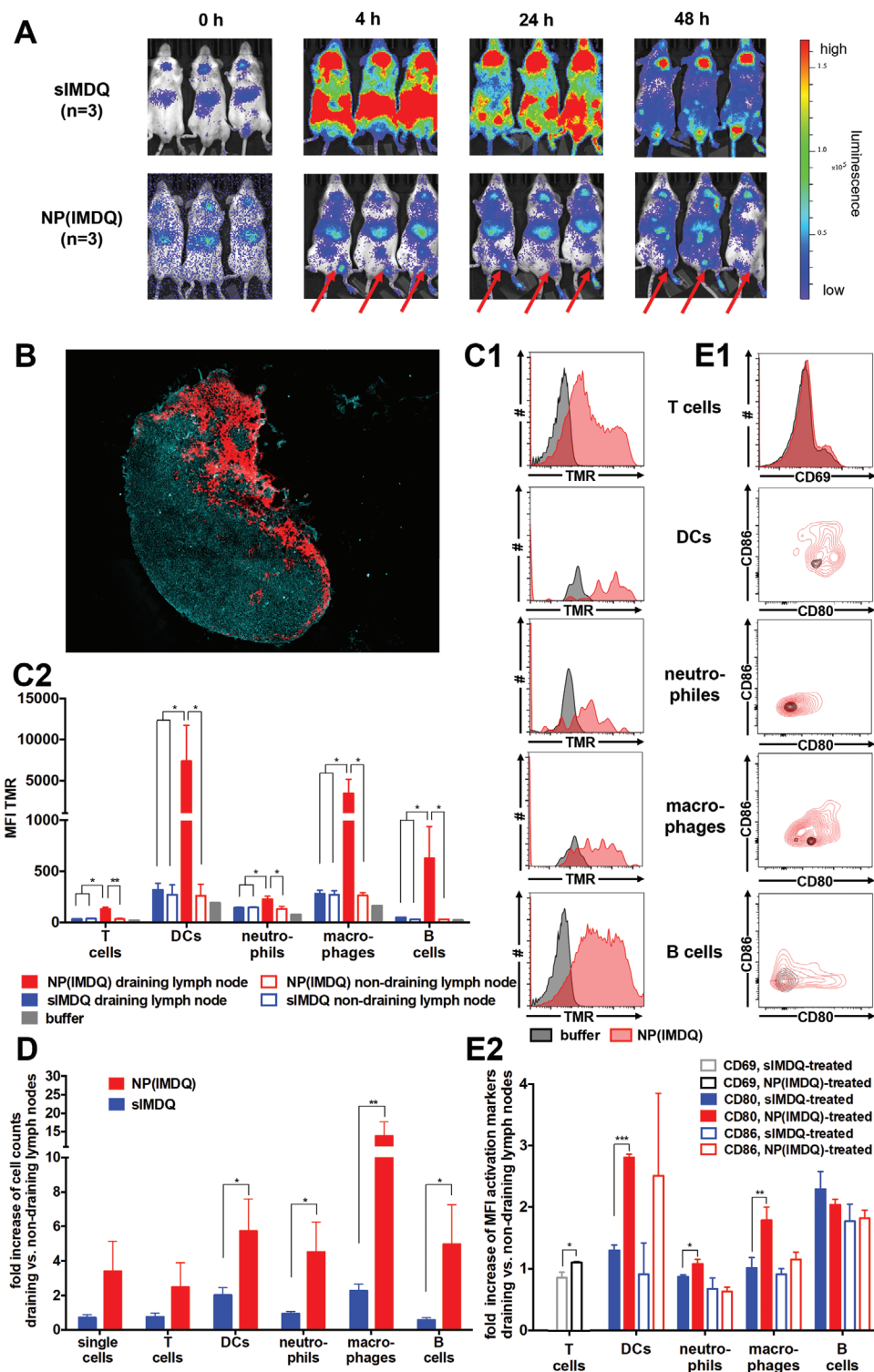
Figure 6. NP(IMDQ)-mediated local activation of draining lymph nodes by subcutaneous footpad injection. A) Visualization of immune activation in IFN-β luciferase reporter (IFN-$\beta^{+/\Delta\beta\text{-luc}}$) mice. In contrast to the small molecule sIMDQ, the immunodrug-loaded nanogels NP(IMDQ) provides a lymph node-focused immune cell activation ($n = 3$). B) Confocal imaging of a draining lymph node tissue section with nanogels (red) arriving in the subcapsular sinus and then spreading over to the medulla. C) Flow cytometric analysis of TMR-labeled NP(IMDQ) uptake in different types of immune cells residing in draining and non-draining lymph nodes, as analyzed by flow cytometry histogram (1) or mean fluorescence intensities (MFI) (2) ($n = 3$). D) Increase of cells of draining versus non-draining lymph nodes by flow cytometric cell count analysis ($n = 3$). E) Additional flow cytometric analysis of maturation marker expression (CD80 and CD86, or CD69 for T cells, respectively) determined by flow cytometry histogram (1) or by mean MFI fold increase (2) of immune cells for draining versus non-draining lymph nodes ($n = 3$; ($^{*}p \leq 0.05$; $^{**}p \leq 0.01$; $^{***}p \leq 0.001$; n.s.: not significant).

Both popliteal lymph nodes, the one drained by the lymph of injection site (draining lymph node), as well as the one of the opposite leg (as non-draining lymph node), were isolated and analyzed for nanogel uptake as well as for stimulation of the residing immune cells. Tissue sections were imaged by confocal microscopy and revealed an accumulation of the TMR-labeled nanogels only in the draining lymph node. The particles seemed to have arrived from the subcapsular sinus and then spread over the medulla (Figure 6B) in analogy to previously reported macromolecular carrier systems.[22,87,88,90]

Additionally, single cell suspensions were prepared from the isolated lymph nodes and analyzed by flow cytometry to identify various types of immune cells (compare Figure S35, Supporting Information). Looking at the TMR-derived fluorescence in each immune cell population, an uptake of dye-labeled nanogels NP(IMDQ) could only be found in the draining and not in the non-draining popliteal lymph node. For the draining lymph node, all immune cells (T cells, dendritic cells (DCs), neutrophiles, macrophages, and B cells) provided TMR-derived fluorescence (Figure 6C; Figure S36, Supporting Information). Interestingly, the internalization in B cells as well as macrophages and especially dendritic cells, which are considered to be most effective for antigen presentation, was most pronounced (Figure 6C2).

We then also looked at the immune stimulatory behavior of the delivered TLR7/8 agonist and first compared the number of cells per lymph node for NP(IMDQ) and sIMDQ treated mice (to each lymph node single cell suspension a defined number of beads was added and referenced during flow cytometry—compare Figure S37, Supporting Information). As the massive systemic immune activation caused an alteration of immune cells for sIMDQ in both lymph nodes (compare Figure S37, Supporting Information), we therefore examined the increase of immune cells for the draining compared with the non-draining lymph node, and we observed that the nanogel locally elevated the number of all immune cells, most significantly the number of neutrophiles, B cells, dendritic cells and especially macrophages (Figure 6D). The latter could probably increase due to an additional infiltration of circulating monocytes from the bloodstream that recognize the exclusive stimulation of the draining lymph node by the nanogel-delivered TLR7/8 agonist.

We next checked for the costimulatory maturation surface markers CD80 and CD86 on these immune cell populations (and CD69 as maturation marker on T cells, respectively). In all cases, their expression levels were increased when sIMDQ or NP(IMDQ) was administered compared to the buffer control (Figure 6E1; Figure S38, Supporting Information). However, only for the NP(IMDQ) sample a difference between draining compared to non-draining lymph node was found. We therefore compared again the increase in maturation markers for the draining versus the nondraining lymph node and confirmed once more that only the IMDQ-loaded nanogel locally maturates these immune cells, most significantly neutrophils, macrophages, and especially dendritic cells (Figure 6E2). These observations reiterate that the biodegradable polycarbonate nanogels deliver the TLR7/8 agonist to the draining lymph node and provide a locally well-defined activation of immune cells while omitting systemic inflammatory off-target effects. Such properties are ideal for instance for vaccination or cancer immunotherapeutic purposes, as demonstrated before for similar but less degradable nanogel carriers.[23,81] All in vivo experiments had been approved by the Ethical Committee of the Faculty of Veterinary Medicine and the Faculty of Bioscience Engineering of Ghent University (No. EC2018/92).

3. Conclusion

In conclusion, we reported on a degradable polycarbonate-based nanogel platform that allows the covalent attachment of highly potent TLR7/8 immunodrugs for transient immune activation. For this purpose, we expanded the concept of using reactive precursor block copolymers for the synthesis of core-crosslinked nanogels to hydrolysable polycarbonate-based polymers. Notably, evaluation of polycarbonate nanogel's degradation behavior by various methods revealed a gradual disintegration within several days at physiological conditions (PBS, pH 6.4–7.4, 37 °C). Moreover, the nanogels' disintegration strongly depends on pH and temperature and they are therefore equipped with an intrinsically limited lifetime once they are applied in biological systems. The desired interplay of the chemical structure and biological outcome was validated by the high tolerability of the degraded material and a decreased immune activation upon degradation. The conjugated imidazoquinoline-based TLR7/8 agonists IMDQ retained their bioactivity in vitro on primary immune cells as well as in vivo. For the latter, a spatiotemporal control of immune cell activation only in the draining lymph node after subcutaneous injection could be verified. Altogether, these features make polycarbonate nanogels a promising carrier system for transient lymph node immune activation applications and, thus, also highly attractive for further development toward vaccination or cancer immunotherapeutic purposes. Due to their intrinsic biodegradability while still providing high chemical control during the fabrication process, these carriers might be highly relevant for improved clinical translational perspectives.

Supporting Information

Supporting Information is available from the Wiley Online Library or from the author.

Conflict of Interest

The authors declare no conflict of interest.

Data Availability Statement

The data that support the findings of this study are available in the supplementary material of this article.

Keywords

[1] T. Ye, Z. Zhong, A. García-Sastre, M. Schotsaert, B. G. De Geest, *Angew. Chem., Int. Ed.* **2020**, *59*, 18885.

[2] U. Sahin, Ö. Türeci, *Science* **2018**, *359*, 1355.

[3] S. Gallucci, M. Lolkema, P. Matzinger, *Nat. Med. (N. Y., NY, U. S.)* **1999**, *5*, 1249.

[4] K. Palucka, J. Banchereau, *Nat. Rev. Cancer* **2012**, *12*, 265.

[5] T. A. Yap, E. E. Parkes, W. Peng, J. T. Moyers, M. A. Curran, H. A. Tawbi, *Cancer Discovery* **2021**, *11*, 1368.

[6] H. Cabral, H. Kinoh, K. Kataoka, *Acc. Chem. Res.* **2020**, *53*, 2765.

[7] A. Marabelle, L. Tselikas, T. de Baere, R. Houot, *Ann. Oncol.* **2017**, *28*, xii33.

[8] S. Champiat, L. Tselikas, S. Farhane, T. Raoult, M. Texier, E. Lanoy, C. Massard, C. Robert, S. Ammari, T. de Baere, A. Marabelle, *Clin. Cancer Res.* **2021**, *27*, 665.

[9] G. M. Lynn, R. Laga, P. A. Darrah, A. S. Ishizuka, A. J. Balaci, A. E. Dulcey, M. Pechar, R. Pola, M. Y. Gerner, A. Yamamoto, C. R. Buechler, K. M. Quinn, M. G. Smelkinson, O. Vanek, R. Cawood, T. Hills, O. Vasalatiy, K. Kastenmüller, J. R. Francica, L. Stutts, J. K. Tom, K. A. Ryu, A. P. Esser-Kahn, T. Etrych, K. D. Fisher, L. W. Seymour, R. A. Seder, *Nat. Biotechnol.* **2015**, *33*, 1201.

[10] M. C. Hanson, M. P. Crespo, W. Abraham, K. D. Moynihan, G. L. Szeto, S. H. Chen, M. B. Melo, S. Mueller, D. J. Irvine, *J. Clin. Invest.* **2015**, *125*, 2532.

[11] M. Saeed, J. Gao, Y. Shi, T. Lammers, H. Yu, *Theranostics* **2019**, *9*, 7981.

[12] X. Zhu, F. Nishimura, K. Sasaki, M. Fujita, J. E. Dusak, J. Eguchi, W. Fellows-Mayle, W. J. Storkus, P. R. Walker, A. M. Salazar, H. Okada, *J. Transl. Med.* **2007**, *5*, 10.

[13] L. Hammerich, T. U. Marron, R. Upadhyay, J. Svensson-Arvelund, M. Dhainaut, S. Hussein, Y. Zhan, D. Ostrowski, M. Yellin, H. Marsh, A. M. Salazar, A. H. Rahman, B. D. Brown, M. Merad, J. D. Brody, *Nat. Med.* **2019**, *25*, 814.

[14] G. Frega, Q. Wu, J. L.e Naour, E. Vacchelli, L. Galluzzi, G. Kroemer, O. Kepp, *Oncoimmunology* **2020**, *9*, 1796002.

[15] L. I. Harrison, C. Astry, S. Kumar, C. Yunis, *J. Clin. Pharmacol.* **2007**, *47*, 962.

[16] P. Savage, V. Horton, J. Moore, M. Owens, P. Witt, M. E. Gore, *Br. J. Cancer* **1996**, *74*, 1482.

[17] P. J. Pockros, D. Guyader, H. Patton, M. J. Tong, T. Wright, J. G. McHutchison, T. C. Meng, *J. Hepatol.* **2007**, *47*, 174.

[18] S. Hamm, S. Rath, S. Michel, R. Baumgartner, *J. Immunotoxicol.* **2009**, *6*, 257.

[19] R. Ella, S. Reddy, W. Blackwelder, V. Potdar, P. Yadav, V. Sarangi, V. K. Aileni, S. Kanungo, S. Rai, P. Reddy, S. Verma, C. Singh, S. Redkar, S. Mohapatra, A. Pandey, P. Ranganadin, R. Gumashta, M. Multani, S. Mohammad, P. Bhatt, L. Kumari, G. Sapkal,

[20] R. Ella, K. M. Vadrevu, H. Jogdand, S. Prasad, S. Reddy, V. Sarangi, B. Ganneru, G. Sapkal, P. Yadav, P. Abraham, S. Panda, N. Gupta, P. Reddy, S. Verma, S. Kumar Rai, C. Singh, S. V. Redkar, C. S. Gillurkar, J. S. Kushwaha, S. Mohapatra, V. Rao, R. Guleria, K. Ella, B. Bhargava, *Lancet Infect. Dis.* **2021**, *21*, 637.

[21] R. Ella, S. Reddy, H. Jogdand, V. Sarangi, B. Ganneru, S. Prasad, D. Das, D. Raju, U. Praturi, G. Sapkal, P. Yadav, P. Reddy, S. Verma, C. Singh, S. V. Redkar, C. S. Gillurkar, J. S. Kushwaha, S. Mohapatra, A. Bhate, S. Rai, S. Panda, P. Abraham, N. Gupta, K. Ella, B. Bhargava, K. M. Vadrevu, *Lancet Infect. Dis.* **2021**, *21*, 950.

[22] L. Nuhn, N. Vanparijs, A. De Beuckelaer, L. Lybaert, G. Verstraete, K. Deswarte, S. Lienenklaus, N. M. Shukla, A. C. D. Salyer, B. N. Lambrecht, J. Grooten, S. A. David, S. De Koker, B. G. De Geest, *Proc. Natl. Acad. Sci. USA* **2016**, *113*, 8098.

[23] L. Nuhn, S. De Koker, S. Van Lint, Z. Zhong, J. P. Catani, F. Combes, K. Deswarte, Y. Li, B. N. Lambrecht, S. Lienenklaus, N. N. Sanders, S. A. David, J. Tavernier, B. G. De Geest, *Adv. Mater.* **2018**, *30*, 1803397.

[24] A. Schudel, D. M. Francis, S. N. Thomas, *Nat. Rev. Mater.* **2019**, *4*, 415.

[25] H. Cabral, J. Makino, Y. Matsumoto, P. Mi, H. Wu, T. Nomoto, K. Toh, N. Yamada, Y. Higuchi, S. Konishi, M. R. Kano, H. Nishihara, Y. Miura, N. Nishiyama, K. Kataoka, *ACS Nano* **2015**, *9*, 4957.

[26] A. Huppertsberg, L. Kaps, Z. Zhong, S. Schmitt, J. Stickdorn, K. Deswarte, F. Combes, C. Czysch, J. De Vrieze, S. Kasmi, N. Choteschovsky, A. Klefenz, C. Medina-Montano, P. Winterwerber, C. Chen, M. Bros, S. Lienenklaus, N. N. Sanders, K. Koynov, D. Schuppan, B. N. Lambrecht, S. A. David, B. G. De Geest, L. Nuhn, *J. Am. Chem. Soc.* **2021**, *143*, 9872.

[27] Y. Chen, S. De Koker, B. G. De Geest, *Acc. Chem. Res.* **2020**, *53*, 2055.

[28] J. Kockelmann, J. Stickdorn, S. Kasmi, J. De Vrieze, M. Pieszka, D. Y. W. Ng, S. A. David, B. G. De Geest, L. Nuhn, *Biomacromolecules* **2020**, *21*, 2246.

[29] R. Duncan, R. Gaspar, *Mol. Pharmaceutics* **2011**, *8*, 2101.

[30] Q. Jin, Y. Deng, X. Chen, J. Ji, *ACS Nano* **2019**, *13*, 954.

[31] P. Schattling, F. D. Jochum, P. Theato, *Polym. Chem.* **2014**, *5*, 25.

[32] M. Wei, Y. Gao, X. Li, M. J. Serpe, *Polym. Chem.* **2017**, *8*, 127.

[33] S. Wilhelm, A. J. Tavares, Q. Dai, S. Ohta, J. Audet, H. F. Dvorak, W. C. W. Chan, *Nat. Rev. Mater.* **2016**, *1*, 16014.

[34] T. Lammers, F. Kiessling, M. Ashford, W. Hennink, D. Crommelin, G. Strom, *Nat. Rev. Mater.* **2016**, *1*, 16069.

[35] S. C. Baetke, T. Lammers, F. Kiessling, *Br. J. Radiol.* **2015**, *88*, 20150207.

[36] B. Amsden, *Macromol. Biosci.* **2021**, *21*, 210085.

[37] Y. Lu, A. A. Aimetti, R. Langer, Z. Gu, *Nat. Rev. Mater.* **2017**, *2*, 16075.

[38] P. Mainil-Varlet, R. Curtis, S. Gogolewski, *J. Biomed. Mater. Res.* **1997**, *36*, 360.

[39] F. Chen, R. Qi, L. D. Huyer, B. G. Amsden, *Polym. Degrad. Stab.* **2018**, *158*, 83.

[40] G. Becker, F. R. Wurm, *Chem. Soc. Rev.* **2018**, *47*, 7739.

[41] J. H. Jung, M. Ree, H. Kim, *Catal. Today* **2006**, *115*, 283.

[42] S. J. Yoon, S. H. Kim, H. J. Ha, Y. K. Ko, J. W. So, M. S. Kim, Y. Il Yang, G. Khang, J. M. Rhee, H. B. Lee, *Tissue Eng., Part A* **2008**, *14*, 539.

[43] E. Lih, C. H. Kum, W. Park, S. Y. Chun, Y. Cho, Y. K. Joung, K.-S. Park, Y. J. Hong, D. J. Ahn, B.-S. Kim, T. G. Kwon, M. H. Jeong, J. A. Hubbell, D. K. Han, *ACS Nano* **2018**, *12*, 6917.

[44] K. Fu, D. W. Pack, A. M. Klibanov, R. Langer, *Pharm. Res.* **2000**, *17*, 100.

[45] S. Tempelaar, L. Mespouille, O. Coulembier, P. Dubois, A. P. Dove, *Chem. Soc. Rev.* **2013**, *42*, 1312.

[46] Z. Zhang, R. Kuijer, S. K. Bulstra, D. W. Grijpma, J. Feijen, *Biomaterials* **2006**, *27*, 1741.

[47] M. Acemoglu, *Int. J. Pharm.* **2004**, *277*, 133.

[48] J. Xu, E. Feng, J. Song, *J. Appl. Polym. Sci.* **2014**, *131*, 39822.

[49] S. Mohajeri, F. Chen, M. de Prinse, T. Phung, J. Burke-Kleinman, D. H. Maurice, B. G. Amsden, *Mol. Pharmaceutics* **2020**, *17*, 1363.

[50] X.-L. Wang, R.-X. Zhuo, L.-J. Liu, F. He, G. Liu, *J. Polym. Sci., Part A: Polym. Chem.* **2002**, *40*, 70.

[51] J. Liu, W. Liu, I. Weitzhandler, J. Bhattacharyya, X. Li, J. Wang, Y. Qi, S. Bhattacharjee, A. Chilkoti, *Angew. Chem., Int. Ed.* **2015**, *54*, 1002.

[52] C. Czysch, C. Medina-Montano, N.-J. K. Dal, T. Dinh, X. Li, Y. Fröder, P. Winterwerber, K. Maxeiner, H.-J. Räder, D. Schuppan, H. Schild, M. Bros, B. Biersack, F. Feranoli, S. Grabbe, L. Nuhn, *Macromol. Rapid. Commun.* **2022**, *43*, 2200095.

[53] H. Ajiro, Y. Takahashi, M. Akashi, *Macromolecules* **2012**, *45*, 2668.

[54] H.-F. Wang, X.-H. Luo, C.-W. Liu, J. Feng, X.-Z. Zhang, R.-X. Zhuo, *Acta Biomater.* **2012**, *8*, 589.

[55] X. Wang, J. Wilhelm, W. Li, S. Li, Z. Wang, G. Huang, J. Wang, H. Tang, S. Khorsandi, Z. Sun, B. Evers, J. Gao, *Nat. Commun.* **2020**, *11*, 5828.

[56] S. Cho, G. S. Heo, S. Khan, A. M. Gonzalez, M. Elsabahy, K. L. Wooley, *Macromolecules* **2015**, *48*, 8797.

[57] A. C. Engler, X. Ke, S. Gao, J. M. W. Chan, D. J. Coady, R. J. Ono, R. Lubbers, A. Nelson, Y. Y. Yang, J. L. Hedrick, *Macromolecules* **2015**, *48*, 1673.

[58] J. Kockelmann, J. Stickdorn, S. Kasmi, J. De Vrieze, M. Pieszka, D. Y. W. Ng, S. A. David, B. G. De Geest, L. Nuhn, *Biomacromolecules* **2020**, *21*, 2246.

[59] M. Talelli, M. Barz, C. J. F. Rijcken, F. Kiessling, W. E. Hennink, T. Lammers, *Nano Today* **2015**, *10*, 93.

[60] A. E. Ekkelenkamp, M. R. Elzes, J. F. J. Engbersen, J. M. J. Paulusse, *J. Mater. Chem. B* **2018**, *6*, 210.

[61] J. K. Oh, R. Drumright, D. J. Siegwart, K. Matyjaszewski, *Prog. Polym. Sci.* **2008**, *33*, 448.

[62] D. P. Sanders, D. J. Coady, M. Yasumoto, M. Fujiwara, H. Sardon, J. L. Hedrick, *Polym. Chem.* **2014**, *5*, 327.

[63] A. C. Engler, J. M. W. Chan, D. J. Coady, J. M. O'Brien, H. Sardon, A. Nelson, D. P. Sanders, Y. Y. Yang, J. L. Hedrick, *Macromolecules* **2013**, *46*, 1283.

[64] M. Eberhardt, R. Mruk, R. Zentel, P. Théato, *Eur. Polym. J.* **2005**, *41*, 1569.

[65] A. Das, P. Theato, *Chem. Rev.* **2016**, *116*, 1434.

[66] D. P. Sanders, K. Fukushima, D. J. Coady, A. Nelson, M. Fujiwara, M. Yasumoto, J. L. Hedrick, *J. Am. Chem. Soc.* **2010**, *132*, 14724.

[67] D. J. Coady, H. W. Horn, G. O. Jones, H. Sardon, A. C. Engler, R. M. Waymouth, J. E. Rice, Y. Y. Yang, J. L. Hedrick, *ACS Macro Lett.* **2013**, *2*, 306.

[68] L. Mespouille, O. Coulembier, M. Kawalec, A. P. Dove, P. Dubois, *Prog. Polym. Sci.* **2014**, *39*, 1144.

[69] P. W. A. Howe, *Prog. Nucl. Magn. Reson. Spectrosc.* **2020**, *118–119*, 1.

[70] A. M. Nyström, B. Fadeel, *J. Controlled Release* **2012**, *161*, 403.

[71] J. Paradise, *AMA J. Ethics* **2019**, *21*, 347.

[72] M. Vert, Y. Doi, K.-H. Hellwich, M. Hess, P. Hodge, P. Kubisa, M. Rinaudo, F. Schué, *Pure Appl. Chem.* **2012**, *84*, 377.

[73] H. Wu, V. Estrella, M. Beatty, D. Abrahams, A. El-Kenawi, S. Russell, A. Ibrahim-Hashim, D. L. Longo, Y. K. Reshetnyak, A. Moshnikova, O. A. Andreev, K. Luddy, M. Damaghi, K. Kodumudi, S. R. Pillai, P. Enriquez-Navas, S. Pilon-Thomas, P. Swietach, R. J. Gillies, *Nat. Commun.* **2020**, *11*, 4113.

[74] E. Boedtkjer, S. F. Pedersen, *Annu. Rev. Physiol.* **2020**, *82*, 103.

[75] C.-H. Chang, J. Qiu, D. O'Sullivan, M. D. Buck, T. Noguchi, J. D. Curtis, Q. Chen, M. Gindin, M. M. Gubin, G. J. W. van der Windt, E. Tonc, R. D. Schreiber, E. J. Pearce, E. L. Pearce, *Cell* **2015**, *162*, 1229.

[76] L. Nuhn, S. Van Herck, A. Best, K. Deswarte, M. Kokkinopoulou, I. Lieberwirth, K. Koynov, B. N. Lambrecht, B. G. De Geest, *Angew. Chem., Int. Ed.* **2018**, *57*, 10760.

[77] N. Leber, L. Kaps, M. Aslam, J. Schupp, A. Brose, D. Schäffel, K. Fischer, M. Diken, D. Strand, K. Koynov, A. Tuettenberg, L. Nuhn, R. Zentel, D. Schuppan, *J. Controlled Release* **2017**, *248*, 10.

[78] L. Nuhn, L. Braun, I. Overhoff, A. Kelsch, D. Schaeffel, K. Koynov, R. Zentel, *Macromol. Rapid Commun.* **2014**, *35*, 2057.

[79] A. Baumann, D. Tuerck, S. Prabhu, L. Dickmann, J. Sims, *Drug Discov. Today* **2014**, *19*, 1623.

[80] K. Rausch, A. Reuter, K. Fischer, M. Schmidt, *Biomacromolecules* **2010**, *11*, 2836.

[81] L. Nuhn, L. Van Hoecke, K. Deswarte, B. Schepens, Y. Li, B. N. Lambrecht, S. De Koker, S. A. David, X. Saelens, B. G. De Geest, *Biomaterials* **2018**, *178*, 643.

[82] V. Durai, K. M. Murphy, *Immunity* **2016**, *45*, 719.

[83] S. Wirtz, C. Becker, M. C. Fantini, E. E. Nieuwenhuis, I. Tubbe, P. R. Galle, H.-J. Schild, M. Birkenbach, R. S. Blumberg, M. F. Neurath, *J. Immunol.* **2005**, *174*, 2814.

[84] F. Fallarino, C. Orabona, C. Vacca, R. Bianchi, S. Gizzi, C. Asselin-Paturel, M. C. Fioretti, G. Trinchieri, U. Grohmann, P. Puccetti, *Int. Immunol.* **2005**, *17*, 1429.

[85] S. Jangra, J. De Vrieze, A. Choi, R. Rathnasinghe, G. Laghlali, A. Uvyn, S. Van Herck, L. Nuhn, K. Deswarte, Z. Zhong, N. N. Sanders, S. Lienenklaus, S. A. David, S. Strohmeier, F. Amanat, F. Krammer, H. Hammad, B. N. Lambrecht, L. Coughlan, A. García-Sastre, B. G. De Geest, M. Schotsaert, *Angew. Chem., Int. Ed. Engl.* **2021**, *60*, 9467.

[86] H. Li, S. Van Herck, Y. Liu, Y. Hao, X. Ding, L. Nuhn, Z. Zhong, F. Combes, N. N. Sanders, S. Lienenklaus, S. D. Koker, S. A. David, Y. Wang, B. G. De Geest, Z. Zhang, *ACS Biomater. Sci. Eng.* **2020**, *6*, 4993.

[87] S. Van Herck, K. Deswarte, L. Nuhn, Z. Zhong, J. P. Portela Catani, Y. Li, N. N. Sanders, S. Lienenklaus, S. De Koker, B. N. Lambrecht, S. A. David, B. G. De Geest, *J. Am. Chem. Soc.* **2018**, *140*, 14300.

[88] J. De Vrieze, B. Louage, K. Deswarte, Z. Zhong, R. De Coen, S. Van Herck, L. Nuhn, C. K. Frich, A. N. Zelikin, S. Lienenklaus, N. N. Sanders, B. N. Lambrecht, S. A. David, B. G. De Geest, *Angew. Chem., Int. Ed.* **2019**, *58*, 15390.

[89] J. Stickdorn, L. Stein, D. Arnold-Schild, J. Hahlbrock, C. Medina-Montano, J. Bartneck, T. Ziß, E. Montermann, C. Kappel, D. Hobernik, M. Haist, H. Yurugi, M. Raabe, A. Best, K. Rajalingam, M. P. Radsak, S. A. David, K. Koynov, M. Bros, S. Grabbe, H. Schild, L. Nuhn, *ACS Nano* **2022**, *16*, 4426.

[90] J. De Vrieze, A. P. Baptista, L. Nuhn, S. Van Herck, K. Deswarte, H. Yu, B. N. Lambrecht, B. G. De Geest, *Adv. Ther.* **2021**, *4*, 2100079.

2203490 (14 of 14)